Vol 18 No 11, November 2009
1674-1056/2009/18(11)/4988-07

Chinese Physics B

© 2009 Chin. Phys. Soc.
and IOP Publishing Ltd

First-principles calculations on the electronic and vibrational properties of β-V_2O_5*

Zhou Bo(周 波), Su Qing(苏 庆), and He De-Yan(贺德衍)†

Department of Physics, Lanzhou University, Lanzhou 730000, *China*

(Received 5 January 2009; revised manuscript received 27 February 2009)

Using a first-principles approach based on density functional theory, this paper studies the electronic and dynamical properties of β-V_2O_5. A smaller band gap and much wider split-off bands have been observed in comparison with α-V_2O_5. The Raman- and infrared-active modes at the Γ point of the Brillouin zone are evaluated with LO/TO splitting, where the symbol denotes the longitudinal and transverse optical model. The nonresonant Raman spectrum of a β-V_2O_5 powder sample is also computed, providing benchmark theoretical results for the assignment of the experimental spectrum. The computed spectrum agrees with the available experimental data very well. This calculation helps to gain a better understanding of the transition from α- to β-V_2O_5.

Keywords: *ab initio*, β-V_2O_5, density functional perturbation theory, Raman spectrum
PACC: 6320, 7830, 7125T

1. Introduction

Vanadium oxides are noted for their rich and diverse structural, physical, and chemical properties. Among these, vanadium pentoxide has long been a subject of great interest for experimental and theoretical investigations and most studies focus on α-V_2O_5, the most stable phase. The β-V_2O_5 is a polymorph of α-V_2O_5 and was first reported in 1977 by Suzuki *et al.*[1] Volkov *et al* [2] and Filonenko *et al* [3] have reported their study on the crystal structure of β-V_2O_5, based on x-ray and neutron powder diffraction. Both polymorphs have a good performance as a positive electrode for lithium batteries. Gallardo-Amores *et al* [4] have measured the resistivities at room temperature (10000 Ω·cm in α-V_2O_5 and 400 Ω·cm in β-V_2O_5), which reveal that β-V_2O_5 is indeed a better electronic conductor than α-V_2O_5, thus β-V_2O_5 is promising for electrochemical application.

The development of highly efficient and accurate *ab initio* algorithms makes reliable electronic structure calculations and geometry optimizations of very complex transition metal oxides feasible. Nowadays, many physical properties of solids and molecules can be calculated and predicted very accurately from first principles.[5,6] Several first-principle studies on vanadium pentoxide have been published.[7−10] To our knowledge, first-principle studies on β-V_2O_5 are rather limited. Gallardo-Amores *et al* [4] have reported their first *ab initio* calculation of β-V_2O_5, mainly on electronic properties. The vibrational properties of β-V_2O_5 are still untouched.

Infrared (IR) and Raman spectroscopy are two standard, sensitive and widely used techniques in material science to detect the occurrence of new phases or structural changes.[11] Recent Raman spectrum studies of the effect of high pressures on the structure of α-V_2O_5 have suggested that a structural transformation to a three-dimensional V_2O_5 network occurs at about 7 GPa.[12,13] No rigid assignment of Raman modes has been achieved. The theoretical prediction of Raman spectra is still of great importance to help understand the experimental results. Recently very efficient linear-response techniques have been proposed which allow one to obtain dynamical matrices at arbitrary wave vectors with a computational effort comparable to the self-consistent calculation for the unperturbed bulk. Unfortunately, there has been no similar study of related quantities such as the phonon dispersion, and Raman spectra on β-V_2O_5 yet. This work presents the first investigation of the vibrational properties of β-V_2O_5 based on density functional perturbation theory (DFPT).[14] The present calculation of lattice vibration modes is in fairly good agreement with the available experimental data.

The paper is organized as follows. Section 2 describes the computational details. In Section 3, we present our results and discussions. Band structure, density of state and zone centre phonons are discussed

*Project supported by the Teaching and Research Award Program for Outstanding Young Teachers in High Education Institutions of MOE, China.
†E-mail: hedy@lzu.edu.cn

in this section. Finally, we summarize our conclusions in Section 4.

2. Method

2.1. Computational details

All the calculations have been performed by using plane waves and norm-conserving pseudopotential as implemented in ABINIT code.[15] Fritz-Haber-Institute (FHI) pseudopotentials, generated by the FHI98PP code,[16] are used in this work. The exchange–correlation energy is evaluated within the local density approximation (LDA) by using Ceperley–Alder homogeneous electron-gas data.[17] Brillouin zone summations of electronic quantities are performed on an 8×8×8 Monkhorst–Pack grid.[18] A plane wave basis set with a cutoff of 60 Hartree is used to expand the electronic wavefunctions. The initial cell parameters and atomic positions of β-V_2O_5 are taken from Ref.[3]. We determine the structural parameters of β-V_2O_5 by relaxing simultaneously the cell shape and the atomic positions. The structural relaxation is conducted by using the Broyden–Fletcher–Goldfarb–Shanno (BFGS) minimization, modified to take into account the total energy as well as the gradients. In the optimized structure reported here, the forces on the atoms are less than 10^{-6} Hartree/Bohr and the stresses on the unit cell are smaller than 10^{-7} Hartree/Bohr^3. After optimization of the crystal structure, we calculate the band structure and other properties of β-V_2O_5.

We also compute the phonons at Γ points, Raman susceptibility tensors within DFPT, using the responses to atomic displacements and homogeneous electric fields. Technical details about DFPT employed in this paper can be found in Ref.[19]–[21]. After balancing the computational consumption and the veracity, the q grid was a 4×4×4 homogeneous grid and the planewave cutoff energy was 60 Hartree.

2.2. Calculation of nonresonant Raman spectrum

Here we briefly outline the formulation that we use for the calculation of Raman intensity. The matrix of interatomic force constants $\tilde{C}$ can be expressed as the sum of an analytical part and a nonanalytical term

$$\tilde{C}_{\kappa\alpha,\kappa'\beta}(q\to 0)=\tilde{C}^{\mathrm{AN}}_{\kappa\alpha,\kappa'\beta}(q=0)+\tilde{C}^{\mathrm{NA}}_{\kappa\alpha,\kappa'\beta}(q\to 0). \tag{1}$$

The analytical part corresponds to the second-order derivative of the energy with respect to an atomic displacement at q=0. The second term is due to the long-range electrostatic interactions in polar crystals. It is the origin of the longitudinal optical (LO) transverse optical (TO) splitting and can be computed from the knowledge of the Born effective charge $Z^*_{\kappa\alpha\beta}$ and the electronic dielectric tensor ε_{ij}. The phonon wavenumber ω_m and eigendisplacements $u_m(k\alpha)$ are solutions of the following generalized eigenvalue problem:

$$\sum_{\kappa',\beta}\tilde{C}_{k\alpha,k'\beta}u_m(k'\beta)=M_k\omega_m^2u_m(k\alpha). \tag{2}$$

The peak intensity of the nonresonant Stokes Raman spectrum can be calculated under the Placzek approximation:[22]

$$I_{mij}=\frac{2\pi\hbar(\omega_{\mathrm{L}}-\omega_m)^4}{c^4\omega_m}\left[n(\omega_m)+1\right](\alpha^m_{ij})^2, \tag{3}$$

$$n(\omega_m)=\frac{1}{\mathrm{e}^{\hbar\omega_m/k_{\mathrm{B}}T}-1}, \tag{4}$$

where I_{mij} is the part of intensity of the mode m, polarized along i and the field along j direction, ω_{L} is the laser wavenumber, ω_m is the wavenumber of the mode m, $n(\omega_m)+1$ is the Bose occupation number, T is the temperature, α^m_{ij} is the Raman susceptibility defined as

$$\alpha^m_{ij}=\sqrt{\Omega_0}\sum_{k,\beta}\frac{\partial\chi^{(1)}_{ij}}{\partial\tau_{k\beta}}u_m(k\beta), \tag{5}$$

where $\chi^{(1)}_{ij}$ is the electronic linear dielectric susceptibility tensor. Ω_0 is the angle of collection in which the outgoing photon is scattered. $\tau_{k\beta}$ is the displacement of the atom k along the β direction from its equilibrium position.

For pure transverse optical phonons, $\partial\chi^{(1)}_{ij}/\partial\tau_{k\lambda}$ can be calculated as follows:[23]

$$\frac{\partial\chi^{(1)}_{ij}}{\partial\tau_{\kappa\lambda}}|_{\varepsilon=0}=-\frac{6}{\Omega_0}E^{\tau_{\kappa\lambda}\varepsilon_i\varepsilon_j}, \tag{6}$$

where $E^{\tau_{\kappa\lambda}\varepsilon_i\varepsilon_j}$ stands for calculation of a mixed third-order derivative of the energy with respect to two electric fields and an atomic displacement under the condition of zero electric field. For longitudinal optical phonons with wave vector $q\to 0$ in a polar crystal, the macroscopic electric field generated by the lattice polar vibration must be taken into account.

$$\frac{\partial\chi^{(1)}_{ij}}{\partial\tau_{\kappa\lambda}}=\frac{\partial\chi^{(1)}_{ij}}{\partial\tau_{\kappa\lambda}}|_{\varepsilon=0}-\frac{8\pi}{\Omega_0}\frac{\sum_l Z^*_{\kappa\lambda l}q_l}{\sum_{l,l'}q_l\varepsilon_{ll'}q_{l'}}\sum_l\chi^{(2)}_{ijl}q_l, \tag{7}$$

where $Z^*_{\kappa\lambda l}$ is the Born effective charge. $\chi^{(2)}_{ijl}$ is the second-order nonlinear optical susceptibility. The third-order derivative of the energy ($E^{\tau_{\kappa\lambda}\varepsilon_i\varepsilon_j}$) can be computed from a straightforward application of the $2n+1$ theorem which has been coded in the ABINIT package. The Raman susceptibility α^m_{ij} can be computed by the ANADDB tool in the ABINIT package.

The peak intensity in Eq.(3) is applicable to single crystals. For the powder sample, the integral intensity is averaged over the possible directions of crystallites.

$$G^{(0)}_m = \frac{1}{3}(\alpha^m_{xx}+\alpha^m_{yy}+\alpha^m_{zz})^2, \tag{8a}$$

$$G^{(1)}_m = \frac{1}{2}[(\alpha^m_{xy}-\alpha^m_{yx})^2+(\alpha^m_{xz}-\alpha^m_{zx})^2 + (\alpha^m_{zy}-\alpha^m_{yz})^2], \tag{8b}$$

$$G^{(2)}_m = \frac{1}{2}[(\alpha^m_{xy}+\alpha^m_{yx})^2+(\alpha^m_{xz}+\alpha^m_{zx})^2 + (\alpha^m_{zy}+\alpha^m_{yz})^2] + \frac{1}{3}[(\alpha^m_{xx}-\alpha^m_{yy})^2+(\alpha^m_{xx}-\alpha^m_{zz})^2 + (\alpha^m_{yy}-\alpha^m_{zz})^2]. \tag{8c}$$

For the 90° and backscattering geometry, the intensity of the powder can be expressed as

$$I^{\text{powder}}_{m||} \propto (\omega_{\text{L}}-\omega_m)^4\frac{1+n(\omega_m)}{30\omega_m}[10G^{(0)}_m+4G^{(2)}_m], \tag{9a}$$

$$I^{\text{powder}}_{m\perp} \propto (\omega_{\text{L}}-\omega_m)^4\frac{1+n(\omega_m)}{30\omega_m}[5G^{(0)}_m+3G^{(2)}_m], \tag{9b}$$

$$I^{\text{powder}}_{m_\text{total}} = I^{\text{powder}}_{m||} + I^{\text{powder}}_{m\perp}, \tag{9c}$$

where $I^{\text{powder}}_{m||}$ and $I^{\text{powder}}_{m\perp}$ correspond to the polarized and depolarized light respectively. Finally, we plot the Raman spectrum by using the following expressions:

$$I^{\text{powder}}_{\text{total}} = \sum_m I^{\text{powder}}_{m_\text{total}}\frac{\Gamma_m}{(\omega-\omega_m)^2+\Gamma^2_m}. \tag{10}$$

The calculated Raman spectrum has a Lorentzian shape. The parameter Γ_m is the damping constant for the mth mode. In this paper, we take Γ_m as a unique number to give the most familiar shape in comparison with the experimental spectrum.

3. Results and discussion

3.1. Geometric structure

The $\beta-V_2O_5$ exhibits monoclinic $P2_1/m$ symmetry with the unit cell $a = 7.114$ Å, $b = 3.572$ Å and $c = 6.285$ Å. In β-V_2O_5, there are 2 six-coordinated vanadium atoms, V1 and V2, within highly distorted VO_6 octahedra as shown in Fig.1. The V atoms in the octahedra are off-centre. The short band distances are V1–O1=1.65 and V2–O3=1.58 Å in octahedra, while the long ones are V1–O2=2.31 and V2–O1=2.30 Å. Full details of the V–O bonds in octahedra are shown in Fig.2. The VO_6 octahedra are linked in pairs. The β-V_2O_5 structure can be described as a build up of infinite chains of such quadruple units, sharing edges along the short b axis. The chains are mutually linked by corner-sharing between two octahedra along the c axis, thus forming two-dimensional layers of the composition V_4O_{10} in planes parallel to (100). The layers are held together by weak forces. The transition process α-V_2O_5 to β-V_2O_5 can be explained by a conversion of a b layer into an a layer in the α-form followed by a compression of the α-V_2O_5 structure along the c-axis.

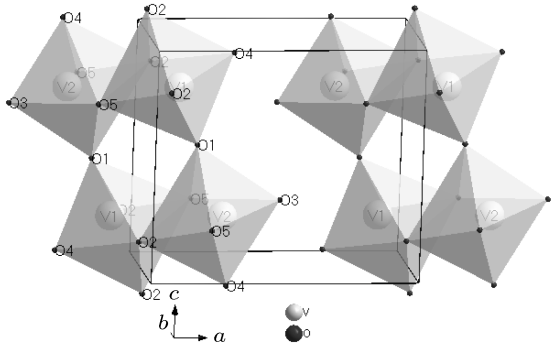


Fig.1. Structure of β-V_2O_5.

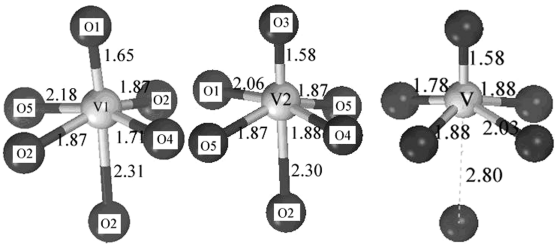


Fig.2. View of $V1O_6$ (left) and $V2O_6$ (middle) coordination polyhedra in β-V_2O_5 and α-V_2O_5(right).

The lattice parameters and atomic positions for β-V_2O_5 are listed in Table 1. There are five structural inequivalent oxygen atoms in β-V_2O_5. We classify them as three kinds like in α-V_2O_5. The O3 should be terminal (vanadyl) oxygen. The O1, O4 are the oxygen bridging two vanadium centres. But O1 and O4 are different in consideration of the V–O–V angle (179° for V1–O1–V2, 118° for V1–O4–V2). O2, O5 are bridging oxygen connected with three vanadium centres. The five structural inequivalent oxygen atoms can be distinguished from the partial density of state in the next section.

Table 1. Fractional coordinates of all inequivalent atoms inside β-V_2O_5. The r_{exp} stands for experimental atomic parameters (Ref.[3]). The r_{opt} is the atomic parameter after the optimization.

lattice parameters	experiment	calculated
a, b, c/Å	7.114, 3.571, 6.284	6.875, 3.602, 6.193
α, β, γ	90.0°, 90.069°, 90.0°	90.0°, 89.942°, 90.0°
inequivalent atoms	r_{exp}	r_{opt}
	V1: 0.0998, 0.25, 0.8103	V1:0.0925, 0.25, 0.8098
	V2: 0.2773, 0.25, 0.2557	V2:0.2826, 0.25, 0.2619
	O1: 0.8241, 0.75, 0.4374	O1:0.8313, 0.25, 0.4493
	O2: 0.9693, 0.25, 0.1464	O2:0.9737, 0.25, 0.1383
	O3: 0.4914, 0.25, 0.3248	O3:0.5096, 0.25, 0.3286
	O4: 0.3012, 0.25, 0.9576	O4:0.3070, 0.25, 0.9609
	O5: 0.1992, 0.75, 0.2627	O5:0.1968, 0.75, 0.2542

3.2. Band structure

The electronic structure of β-V_2O_5 is characterized by energy bands and band states inside the irreducible part of the monoclinic Brillouin zone (BZ) as sketched in Fig.3. All energy values are given relative to the Fermi level so that negative energies refer to valence bands while positive values characterize conduction bands. The right part of Fig.4 displays the total density of states (TDOS) where no energy broadening is applied. The general features of the band structure are similar to that of α-V_2O_5. The calculated direct energy gap at Γ is 1.87 eV. The indirect gap corresponding to a transition from E to Γ is 1.66 eV. The valence band is found to have a width of 5.6 eV which is almost the same as that of α-V_2O_5 obtained from

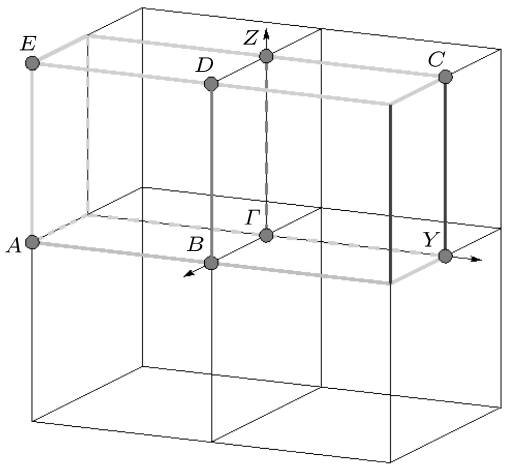


Fig.3. Brillouin zone of the monoclinic β-V_2O_5 lattice with high-symmetry points labelled accordingly.

angle-resolved ultraviolet photoemission spectroscopy in Ref.[10]. Along the $\Gamma - B$ (parallel to the x axis) the dispersion of the bands is small and the electrons are well localized. There are still two split-off conduction bands at about 2 eV above the Fermi level. But it is much wider than that in α-V_2O_5. This broad split-off conduction band indicates a higher carrier mobility.

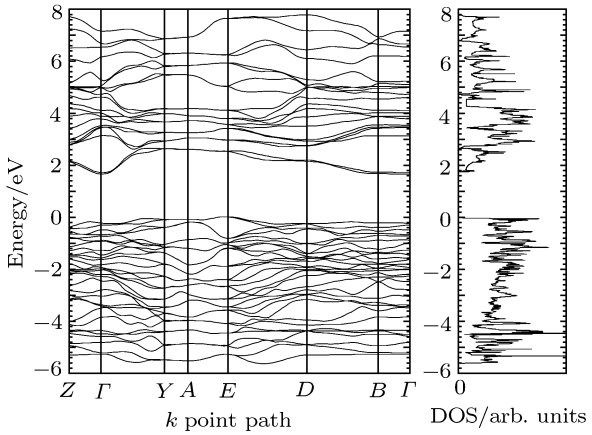


Fig.4. Band structure and TDOS of β-V_2O_5. All energies are taken relative to the Fermi energy.

Figure 5 shows a decomposition of the calculated TDOS for β-V_2O_5 into atom projected contributions (partial density of state, PDOS). There are seven PDOS corresponding to seven inequivalent atoms in β-V_2O_5. The valence band of β-V_2O_5 consists mainly of oxygen 2p states, whereas the conduction band mainly comprises unoccupied vanadium 3d states. The PDOS reflects a substantial degree of hybridization between oxygen 2p and vanadium 3d states.

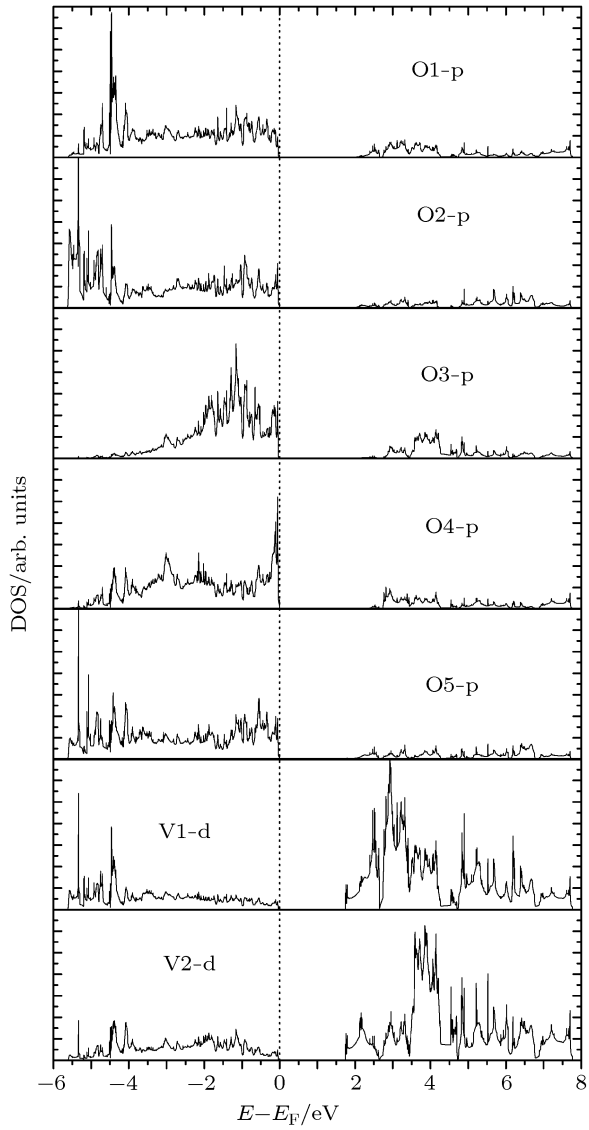


Fig.5. Projected density of state of β-V_2O_5. The ranges of the y axis are the same.

3.3. Vibrational properties of β-V_2O_5

First we present the phonon frequencies at the Γ point. The calculated mode frequencies are summarized in Table 2. Since there are 14 atoms in the unit cell, there are 39 optical modes ($\Gamma_{\rm opt}$) and 3 acoustic modes ($\Gamma_{\rm acoustic}$). From the factor group analysis for this unit cell (C_{2h}), the zone-centre optical modes at the Γ point are classified into the following:

$$\Gamma_{\rm opt} = 14A_g \oplus 7B_g \oplus 6A_u \oplus 12B_u,$$

$$\Gamma_{\rm acoustic} = A_u \oplus 2B_u.$$

All the g modes are Raman active, while all the u modes are infrared active. Therefore 21 Raman and 18 infrared modes are expected for the β-V_2O_5 compound under study. From the crystal symmetry, the one-dimensional modes B_g and A_u are the atomic motions parallel to the b axis, while the A_g and B_u modes are those perpendicular to it. These wavenumbers in Table 2, however, cannot be compared directly with experimental values since no experimental inelastic neutron scattering data are presently available. Also, Raman and IR spectra of single crystal β-V_2O_5 are hard to obtain because of the experimental limitations.

Table 2 also summarizes the computed frequencies of the TO and LO optic modes of A_u and B_u symmetry. LO–TO splittings are found only in the infrared-active A_u and B_u modes. The largest splitting is found in the A_u mode. The LO-TO splitting of the A_u mode at 697 cm^{-1} is 165.4 cm^{-1}, and the mode at 551 cm^{-1} is 143.9 cm^{-1}. The large splitting mainly attributes to the out of plane vibration of O2, O5 (the oxygen bridging three vanadium centres). The mode at 697 cm^{-1} can be described as the stretching of O2 layers against O5 layers along the y direction. The mode at 551 cm^{-1} can be described as the stretching of oxygen layers against vanadium layers along the y direction.

Table 2. Calculated eigenwavenumbers of the phonon modes at the centre of the Brillouin zone for β-V_2O_5. The triply-degenerated acoustic mode with zero frequencies is not listed. All wavenumbers are given in cm^{-1}. The symbol TO (LO) denotes transverse (longitudinal) optical mode.

mode	energy	mode	energy (TO/LO)
A_g	127.7	A_u	148.1/148.7
	186.9		208.4/208.7
	222.0		257.9/281.7
	248.9		286.6/326.7
	277.2		551.0/694.9
	314.3		697.6/863.0
	331.4	B_u	193.2/197.1
	368.5		243.7/250.8
	458.1		273.4/276.3
	494.7		281.4/331.4
	610.8		342.1/367.9
	786.6		368.0/400.4
	971.7		484.2/491.6
	1079.4		540.3/568.9
B_g	124.2		594.4/630.9
	186.4		783.3/873.0
	213.3		957.7/1031.4
	270.9		1072.8/1100.0
	292.8		–
	612.6		–
	752.1		–

To give an intuitive picture, we calculated the single crystal powder sample Raman spectrum of β-V_2O_5, as shown in Fig.6. Raman peaks are labelled according to Table 2. The largest intensities are obtained for the highest A_g mode (at 971 cm^{-1}). In the low wavenumber region (about 100–300 cm^{-1}) and at about 600 cm^{-1}, several peaks are merged into one peak because of the very close peak centres.

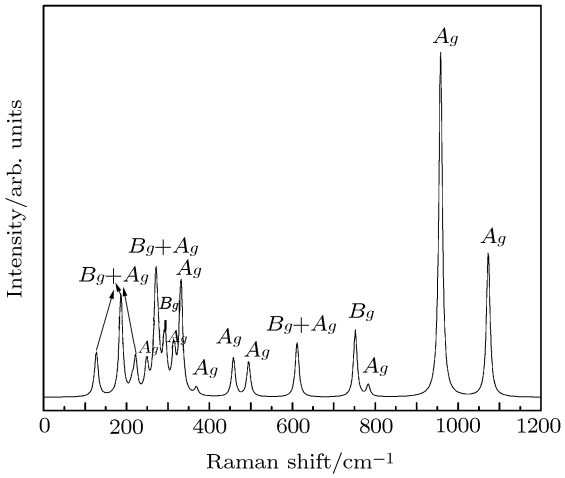


Fig.6. Simulated Raman spectrum of single crystal powder β-V_2O_5 sample. '$B_g + A_g$' means that there exist two Raman modes with very close wavenumbers.

In the Raman spectra of α-V_2O_5, the Raman mode at 997 cm^{-1} is most important, because it is unique and not present in lower oxides of vanadium. It concerns the stretching of the V=O bond. The red shift of this mode is associated with the increase of the short V=O bond and the decrease of the interlayer V–O distance. The downshift of the 997 cm^{-1} mode has been observed by many researchers[12,13] during the α to β phase transition. Inspection of the phonon eigendisplacement vectors allows us to point out the distortion pattern. In our calculation, the peak at 970 cm^{-1} corresponds to stretching of the O1–V1 bond which can be considered as the elongated V=O bond in α-V_2O_5. This is consistent with other researchers. Moreover, our calculations indicate that there is a small peak at (1070 cm^{-1}) which corresponds to stretching of the V2–O3 bond. Judging from the bond length, this Raman mode is similar to the highest V=O mode in α-V_2O_5. This indicates that, during the high pressure condition, the Raman peak at 997 cm^{-1} splits into two lines, one shifting toward a lower wavenumber with high intensity and one staying unmoved with the intensity becoming much smaller. The downshifted A_g mode can be used as the characteristic peak in the study of β-V_2O_5 concerned compounds.

Comparison of the infrared spectra of the α and β phases indicates that additional new bands are presented in the β polymorph at 780 and 950 cm^{-1}. The two new infrared modes are remarkably well reproduced by our calculation.

4. Conclusions

We have investigated the electronic and vibrational properties of β-V_2O_5, mainly from the standpoint of a first-principles calculation. Rather detailed pictures of the geometric and electronic structures of β-V_2O_5 have been obtained. The obtained band gap is 1.66 eV smaller than that of α-V_2O_5. The split-off bands still exist, but are wider than that in α-V_2O_5 and are very close to the above conductive bands. A higher carrier mobility is expected.

A nonresonant Raman spectrum of a β-V_2O_5 powder sample is also computed. Comparability and consistency have been found, comparing with the available Raman experimental data. Our calculation is helpful in the understanding of Raman spectra diversification within the α- to β-V_2O_5 transition process.

Acknowledgements

The computer power is provided by the High Performance Computing Center of Lanzhou University.

References

[1] Suzuki T, Saito S and Arakawa W 1997 *J. Non-Cryst. Solids* **24** 355
[2] Volkov V L, Golovkin V G, Fedyukov A S and Zaynulin Yu G 1998 *Izv. Akad. Nauk. SSSR Neory. Mater.* **24** 355
[3] Filonenko V P, Sundberg M, Werner P E and Zibrov I P 2004 *Acta Crystallographica Section* B **60** 375
[4] Gallardo-Amores J M, Biskup N, Amador U, Persson K, Ceder G, Morán E and Arroyo y de Dompablo M E 2007 *Chem. Mater.* **19** 5262
[5] Li C B, Li M K, Yin D, Liu F Q and Fan X J 2005 *Chin. Phys.* **14** 2287
[6] Sun B and Zhang P 2008 *Chin. Phys.* B **17** 1364
[7] Zhou B and He D Y 2008 *J. Raman Spectrosc.* **39** 1475

[8] Monssanek R J O, Mocellin A, Abbate M, Searle B G, Fonseca P T and Morikawa E 2008 *Phys. Rev.* B **77** 075118
[9] Eyert V and Hock KH 1998 *Phys. Rev.* B **57** 12727
[10] Chakrabarti A, Hermann K, Druzinic R, Witko M, Wagner F and Petersen M 1999 *Phys. Rev.* B **59** 10583
[11] Su Q, Liu X Q, Ma X Q, Guo Y P and Wang Y Y 2008 *J Solid State Electrochem.* **12** 919
[12] Grzechnik A 1998 *Chem. Mater.* **10** 2505
[13] Loa I, Grzechnik A, Schwarz U, Syassen K, Hanfland M and Kremer R K 2001 *J. Alloys. Compd.* **317-318** 103
[14] Baroni S, de Gironcoli S, Dal Corso A and Giannozzi P 2001 *Rev. Mod. Phys.* **73** 515
[15] Gonze X, Beuken J M, Caracas R, Detraux F, Fuchs M, Rignanese G M, Sindic L, Verstraete M, Zerah G, Jollet F, Torrent M, Roy A, Mikami M, Ghosez Ph, Raty G M and Allan D C 2002 *Comput. Mater. Sci.* **25** 478
[16] Fuchs M and Scheffler M 1999 *Comput. Phys. Commun.* **119** 67
[17] Ceperley D M and Alder B J 1980 *Phys. Rev. Lett.* **45** 566
[18] Monkhorst H J and Pack H J 1976 *Phys. Rev.* B **13** 5188
[19] Gonze X 1995 *Phys. Rev.* A **52** 1096
[20] Gonze X 1997 *Phys. Rev.* B **55** 10337
[21] Gonze X and Lee C 1997 *Phys. Rev.* B **55** 10355
[22] Born M and Huang K 1969 *Dynamical Theory of Crystal Lattices* (Oxford: University Press)
[23] Veithen M, Gonze X and Ghosez Ph 2005 *Phys. Rev.* B **71** 125107